# Spectroscopy of the electric-quadrupole transition $^2S_{1/2}(F=0)-{}^2D_{3/2}(F=2)$ in trapped $^{171}Yb^+$

Chr. Tamm,* D. Engelke, and V. Bühner
*Physikalisch-Technische Bundesanstalt (PTB), Bundesalle 100, D-38023 Braunschweig, Germany*
(Received 3 September 1999; published 10 April 2000)

We experimentally demonstrate laser spectroscopy of the electric-quadrupole transition $6s\ ^2S_{1/2}-5d\ ^2D_{3/2}$ of a single trapped $^{171}$Yb ion. The probed transition has a natural linewidth of 3.1 Hz, and is at a wavelength of 435.5 nm. A $^{171}$Yb ion is laser cooled to the range of the Doppler limit in a radio-frequency Paul trap. The $F=0-F'=2$, $m_{F'}=0$ hyperfine component of the $^2S_{1/2}-{}^2D_{3/2}$ transition is excited by a laser source whose frequency is controlled by an optical reference cavity of high intrinsic stability. The recoilless carrier component of the vibrational sideband spectrum is resolved with a minimum linewidth of approximately 80 Hz, corresponding to a fractional frequency resolution of $1.2\times10^{-13}$. This resolution limit is attributed to laser frequency instability. The effective decoherence rates of the residual ion motion are inferred from the observation that the axial and two radial low-frequency first-order secular-vibration sidebands show minimum linewidths in the range of 0.2–1 kHz. Prospects for an optical frequency standard based on the investigated atomic system are discussed.

PACS number(s): 32.80.Pj, 42.50.Lc

## I. INTRODUCTION

Ion traps are a unique basis for precision spectroscopy and quantum state control experiments, because individual atomic systems can be confined over long times with only small and well-defined perturbations [1]. A single laser-cooled ion stored in a suitably dimensioned radio-frequency quadrupole trap typically satisfies the Lamb-Dicke criterion in the optical wavelength range, so that the phase coherence between externally applied radiation fields and atomic internal state evolution is not significantly reduced by linear Doppler-effect frequency shifts [2].

The alkalilike $^2S_{1/2}-{}^2P_{1/2}$ resonance transitions of the singly ionized group-II elements, and of ionic mercury ($Hg^+$) and ytterbium ($Yb^+$) permit high fluorescence scattering rates. This is of advantage in particular in experiments which rely on efficient laser cooling of a trapped ion to the Doppler limit, and on the detection of individual quantum jumps through the electron shelving technique [3]. The ions $^{199}Hg^+$ and $^{171}Yb^+$ have a nuclear spin of $I=\frac{1}{2}$, so that $m_F=0-m_{F'}=0$ reference transitions with a vanishing low-field linear Zeeman effect frequency shift are available in level systems with relatively simple hyperfine and magnetic-sublevel structure. Therefore, $^{199}Hg^+$ and $^{171}Yb^+$ are an attractive choice for high-resolution spectroscopy investigations and for frequency standards in the microwave and optical frequency range [4–12].

Optical spectroscopy with linewidths in the sub-kHz range has been demonstrated for a few alkalilike ions including $^{199}Hg^+$, and for $In^+$ [12–16]. In this paper, we report experiments that demonstrate high-resolution optical spectroscopy on trapped $^{171}Yb^+$. The probed transition is the electric-quadrupole transition from the $F=0$ ground-state hyperfine level to the metastable level $5d\ ^2D_{3/2}(F=2)$. The transition is at a wavelength of 435.5 nm [17]. Lifetime measurements of the $^2D_{3/2}$ state indicate a natural linewidth of 3.1 Hz [18]. Our experiments extend earlier work on laser cooling schemes for trapped $Yb^+$ [19], on the excitation of the transitions from the ground state to the levels $^2D_{5/2}$ and $^2F_{7/2}$ in $Yb^+$ isotopes without hyperfine structure [20], and on the detection of quantum jumps to the $^2D_{3/2}(F=2)$ level in $^{171}Yb^+$ [21]. One distinguishing feature of the spectroscopic scheme investigated here is that the rate of transitions to the long-lived metastable state $^2F_{7/2}$ is negligibly small. Hence the laser cooling and probe excitation cycle is not slowed down by dwell times in the $^2F_{7/2}$ state.

In our experiments a single $^{171}Yb$ ion is prepared and laser cooled in a radio-frequency trap, so that the Lamb-Dicke condition is satisfied for optical excitation. During intervals when the cooling radiation is blocked, a tunable narrow-bandwidth laser source excites the transition to the $F=2$, $m_F=0$ sublevel of the $^2D_{3/2}$ state. The probability of quantum jumps to this state is registered as a function of the optical excitation frequency. The applied probe radiation pulses are short compared to the natural lifetime of the $^2D_{3/2}$ state; the effective pulse area is typically in the range of $\pi/2$ to $\pi$. Under these conditions one expects that observed resonance line shapes are essentially free of saturation features, and that the lower linewidth limit is inversely proportional to the pulse length [22]. In the present experiment, the recoilless carrier resonance of the vibrational spectrum of the probed transition is resolved with a minimum linewidth of approximately 80 Hz (full width at half maximum). This resolution limit appears to be determined by laser frequency instability. The resulting ratio of linewidth to transition frequency is $1.2\times10^{-13}$, which is comparable to the most favorable frequency resolution values reported so far in microwave and optical atomic spectroscopy [10,12].

Heating and motional decoherence effects in radiofrequency ion traps have received increasing attention in the context of experiments related to the preparation and manipulation of nonclassical motional states [23–25]. The motional relaxation of trapped ions is also of interest in high-resolution spectroscopy investigations because a significant heating during probe intervals would give rise to increased

*Electronic address: christian.tamm@ptb.de

 

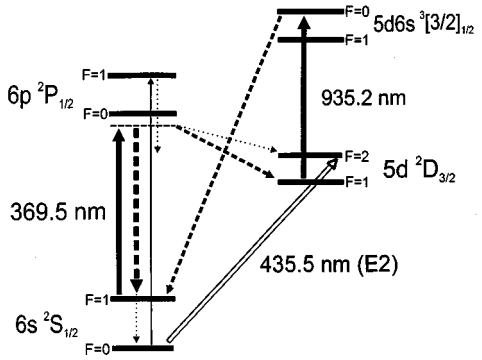


FIG. 1. Partial energy-level system of $^{171}Yb^+$, showing the applied optical excitation (full arrows) and experimentally relevant spontaneous decay paths (broken arrows). The hyperfine splittings of the atomic energy levels are not drawn to scale. The corresponding splitting frequencies are (see Refs. [9,21]) $\Delta_s \cong 12.6$ GHz, $\Delta_P \cong 2.1$ GHz, $\Delta_D \cong 0.86$ GHz, and $\Delta_{[3/2]} \cong 2.5$ GHz.

confinement-related transition frequency shifts. In our experiments, an upper limit of the single-ion heating rate is inferred from observations on the relative strength of the secular-vibration sidebands of the $^2S_{1/2}(F=0)-^2D_{3/2}(F=2)$ transition for different time delays between cooling and probing. Since the Lamb-Dicke condition is satisfied and the probed residual ion motion is thermal, the effective decoherence rates of axial and radial secular vibration can be inferred from the broadening of the secular-vibration sidebands relative to the carrier resonance [5]. We find that one of the radial sidebands produced by a single trapped $^{171}Yb$ ion can be resolved with a minimum linewidth of 0.2 kHz, which is in the range of the frequency resolution of the performed measurement. The other radial and axial sidebands show minimum linewidths in the range of 1 kHz. The observation that the two radial sidebands, which are nearly frequency degenerate independent of the trap potential, show significantly different linewidths suggests some conclusions on the relevant sources of motional decoherence in the employed trap system.

## II. OPTICAL-EXCITATION AND MEASUREMENT SCHEME

The employed optical-excitation scheme and the relevant section of the energy-level system of $^{171}Yb^+$ is illustrated in Fig. 1. A number of related atomic and experimental parameters are listed in Table I. For optical detection and laser cooling, the $^2S_{1/2}-^2P_{1/2}$ resonance transition of $^{171}Yb^+$ is excited by a linearly polarized traveling-wave laser field tuned to the low-frequency wing of the quasicycling $F=1-F=0$ hyperfine component. Under the conditions of the experiment, the fluorescence photon scattering rate of a cooled, resonantly excited ion is in the range of $R \approx 10^7\ s^{-1}$ which is well below the saturation limit given by $\gamma_P/2 \approx 7 \times 10^7\ s^{-1}$. In order to reduce optical pumping to nonabsorbing superpositions of magnetic sublevels in the $F=1$ ground state, a Larmor precession frequency of order $R/(2\pi)$ is introduced by a static magnetic field oriented at an oblique angle with the polarization of the cooling laser field.

Nonresonant excitation to the $^2P_{1/2}(F=1)$ level leads to hyperfine pumping to the $F=0$ ground state. Neglecting numerical factors due to relative hyperfine transition probabilities, the hyperfine pumping rate is approximately given by $r_H \approx R(\gamma_P/4\pi\Delta_P)^2 \approx 3 \times 10^2\ s^{-1}$. As indicated in Fig. 1, ground-state hyperfine pumping is compensated for during laser cooling by additional resonant excitation $^2S_{1/2}(F=0)-^2P_{1/2}(F=1)$. The rate of spontaneous transitions to the metastable level $^2D_{3/2}(F=1)$ is in the range of $\alpha R \approx 7 \times 10^4\ s^{-1}$ where $\alpha \cong 7 \times 10^{-3}$ is the branching probability for spontaneous transitions $^2P_{1/2}-^2D_{3/2}$ [26]. The $^2D_{3/2}(F=1)$ level is coupled to the $5d6s\ ^3[3/2]_{1/2}(F=0)$ level using excitation at $\lambda = 935.2$ nm. From this level, $^{171}Yb$ ions rapidly decay to the $F=1$ ground state [19,21]. Spontaneous dipole and electric-quadrupole transitions from the energy levels shown in Fig. 1 to the metastable levels $^2D_{5/2}$ and $^2F_{7/2}$ are forbidden by parity and angular-momentum selection rules.

The present experiment is based on the excitation of the electric-quadrupole transition $^2S_{1/2}(F=0)-^2D_{3/2}(F=2)$ of $^{171}Yb^+$. Quantum jumps to the $^2D_{3/2}(F=2)$ state lead to

TABLE I. Spectroscopic and trap parameters. Indicated wavelength values are vacuum wavelengths; natural linewidth values (full width at half maximum) are derived from measured spontaneous decay rates as given in the literature (see Ref. [21]); $\hbar$ is the Planck constant, $k_B$ the Boltzmann constant, $m$ the atomic mass, and $\theta$ the angle between the trap axis and propagation direction of probe laser field.

| | |
|---|---|
| Wavelength and natural linewidth, | $\lambda \cong 369.527$ nm; |
| $^{171}Yb^+$ resonance transition $^2S_{1/2}(F=1)-^2P_{1/2}(F=0)$ | $\gamma_P/(2\pi) \cong 23$ MHz |
| Wavelength and natural linewidth, | $\lambda \cong 435.519$ nm; |
| probed $^{171}Yb^+$ quadrupole transition $^2S_{1/2}(F=0)-^2D_{3/2}(F=2)$ | $\gamma_D/(2\pi) \cong 3.1$ Hz |
| One-dimensional kinetic temperature at Doppler cooling limit | $T_D = \hbar\gamma_P/(2k_B) \cong 0.55$ mK |
| Axial ($z$) and radial ($r$) secular-oscillation frequencies (typical trap operating conditions) | $\omega_z/(2\pi) \cong 0.86$ MHz; $\omega_{r1}/(2\pi) \cong \omega_{r2}/(2\pi) \cong 0.73$ MHz |
| Mean vibrational quantum number of axial secular oscillation at $T_D$ | $\langle n_z\rangle_D = (\gamma_P/\omega_z - 1)/2 \cong 13$ |
| Axial Lamb-Dicke parameter at $\lambda = 435.5$ nm | $\eta_z = (2\pi/\lambda)[\hbar/(2m\omega_z)]^{1/2} \cong 0.084$ |
| Relative intensity of first-order axial secular-oscillation sideband at $T_D$ | $(I_z/I_o)_D \cong \langle n_z\rangle_D \eta_z^2 \cos^2\theta \cong 0.092 \cos^2\theta$ |

detectable intervals of vanishing resonance fluorescence only if this level is not rapidly depleted by the laser cooling excitation. The dwell times in the $^2D_{3/2}(F=2)$ state can be reduced in particular by nonresonant excitation at $\lambda = 935.2$ nm to the level $^3[3/2]_{1/2}(F=1)$. The corresponding transition rate is, however, smaller than the natural decay rate $\gamma_D \cong 19\ s^{-1}$ when the intensity of the $\lambda = 935.2$ nm radiation does not largely exceed the resonant saturation intensity of the $^2D_{3/2}-{}^3[3/2]_{1/2}$ transition [21]. The rate at which the $^2D_{3/2}(F=2)$ state is populated during laser cooling is also of interest since it determines the sensitivity with which small excitation rates on the $^2S_{1/2}(F=0)-{}^2D_{3/2}(F=2)$ transition can be detected. During cooling, population of the $^2D_{3/2}(F=2)$ level is caused predominantly by nonresonant excitation to the $^2P_{1/2}(F=1)$ level, and subsequent spontaneous decay [21]. Under the conditions of the experiment, the corresponding transition rate is in the range of $\alpha r_H \approx 2\ s^{-1}$.

The absorption spectrum of the $\lambda = 435.5$ nm $^2S_{1/2}(F=0)-{}^2D_{3/2}(F=2)$ transition is probed using a measurement cycle as follows. (i) For fluorescence detection and cooling, resonance and hyperfine repumping light fields at $\lambda = 369.5$ nm and light at $\lambda = 935.2$ nm are admitted to the trap. (ii) The hyperfine repumping field is switched off in order to prepare the ion in the $F=0$ ground state. (iii) Light at $\lambda = 369.5$ and 935.2 nm is blocked, and a single rectangular pulse of $\lambda = 435.5$ nm radiation is applied. (iv) Next fluorescence detection and cooling interval. In cycles where an abrupt stop of the fluorescence emission during interval (ii) indicates that preparation in the $F=0$ ground state is likely, the fluorescence signal is registered again at the start of the following cooling interval. The ion is assumed to be in the $^2D_{3/2}(F=2)$ state if the photon number detected in a time interval small compared to $1/\gamma_D$ is below a threshold value; occupation of the ground state is assumed if the threshold is exceeded. In the latter case, the most probable number of detected fluorescence photons is several times larger than the threshold value under the realized experimental conditions [27,28].

The number $N$ of quantum jumps to the $^2D_{3/2}(F=2)$ state which are observed in a given number of measurements $M$ is recorded and displayed as a function of the optical excitation frequency at $\lambda = 435.5$ nm. If the fluctuation of the observed values of $N$ is determined by the quantum projection noise of the energy state measurement, the variance of $N$ is given by $(\Delta N)^2 = Mp(1-p)$ [27]. Here $p = \langle N \rangle / M$ is the probability that the ion is found in the $^2D_{3/2}(F=2)$ state, with $\langle N \rangle$ denoting the statistical average of $N$.

The probability $p$ that the trapped ion is found in the $^2D_{3/2}(F=2)$ state during state detection does not exactly reflect the absorption probability associated with the probe excitation at $\lambda = 435.5$ nm. According to the estimate of nonresonant excitation rates given above, there is a probability of order $\alpha$ that the ion is prepared in the $^2D_{3/2}(F=2)$ state rather than in the $F=0$ ground state during interval (ii). One thus expects a background quantum jump probability of order $p \approx \alpha$ if no resonant excitation is applied during interval (iii), and the probability of spontaneous decay before state detection is negligible. If the $^2S_{1/2}(F=0)-{}^2D_{3/2}(F=2)$ transition is excited by a resonant $\pi$ pulse, $p$ assumes its maximum value. Taking into account stimulated and spontaneous transition probabilities from the $^2D_{3/2}(F=2)$ level to the ground state, one expects that the maximum value of $p$ is always smaller than 1 and lies in the range of $p \leqslant 1-\alpha$.

## III. EXPERIMENTAL SETUP

### A. Trap

The experiment employs a cylindrically symmetric rf quadrupole trap whose ring electrode diameter is 1.4 mm. In order to minimize higher-order multipole components of the trap field, a conical trap electrode design is used [29]. Typically a 16-MHz rf voltage of several hundred V amplitude, and a constant voltage in the range of 15 V, are applied to the trap ring electrode in order to obtain a nearly spherically symmetric pseudopotential with axial and radial secular-oscillation frequencies in the range of 0.8 MHz (see Table I). Trap voltage amplitude fluctuations have a relative magnitude of less than $10^{-4}$ for time intervals of less than 10 s. Ions are loaded by activating an oven filled with isotopically enriched $^{171}$Yb and an electron-emitting filament. The trap is mounted in a quartz glass cell evacuated to a pressure of less than $10^{-9}$ mbar. Typical storage times for single ions are in the range of ten days. Extended periods without fluorescence scattering which can be attributed to population of the $^2F_{7/2}$ state or to molecular-ion formation [30] occurred at a rate in the range of 0.1 $h^{-1}$ during the experiments described here. Over a period of two years, the rate varied between virtually zero and peak values in the range of 1 $h^{-1}$ without correlation to the indicated background gas pressure. The observed behavior might be due to temporally changing gas adsorption and emission properties of parts of the trap setup which give rise to gas density variations in the confinement volume without significantly changing the average background gas pressure.

As indicated in Fig. 2, laser fields at $\lambda = 369.5$, 935.2, and 435.5 nm are directed collinearly through the trap at an angle of $\theta \cong 55°$ with the trap axis. Beam diameters at trap center are in the range of 20–50 $\mu$m. The fluorescence emission is collected in a direction perpendicular to the laser beam propagation direction. An estimated fraction of 0.1% of the scattered fluorescence photons is detected by a phomultiplier tube operated in the counting mode.

After ion loading, constant voltages are applied to oven and electron source in order to compensate for the radial components of the static electric stray field at trap center. Imaging photodetection with a spatial resolution of a few micrometers is used to detect and minimize the stray-field-induced changes in the equilibrium ion position which occur if the radial pseudopotential depth is strongly reduced [31]. In this way, the radial compensation voltages are adjusted with an estimated uncertainty of a few percent. The axial stray field and axial asymmetries of the rf trap field are compensated for by a constant voltage difference between the trap endcap electrodes. The axial compensation field is adjusted such that the relative strength of sidebands at the frequency of the trap field is reduced to less than 10% in the

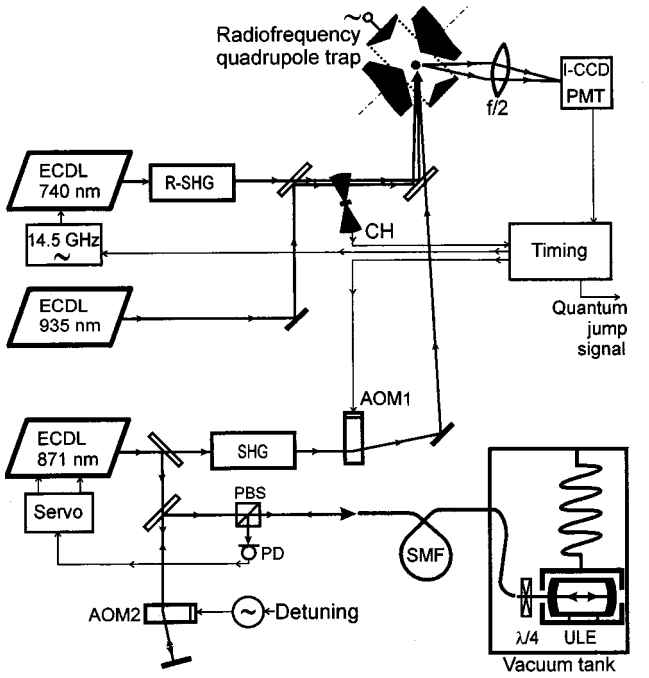


FIG. 2. Experimental scheme. ECDL, extended-cavity diode laser; (R-)SHG, (resonant) second-harmonic generation; CH, chopper wheel; AOM, acousto-optic modulator; PBS, polarizing beamsplitter; SMF, single-mode optical fiber; PD, photodetector; PMT, photomultiplier tube; I-CCD, intensified camera system. For further details, see the text.

excitation spectrum of the $^2S_{1/2}(F=1)-{}^2P_{1/2}(F=0)$ cooling transition.

### B. Lasers

A frequency-doubled extended-cavity semiconductor diode laser excites the $^{171}\mathrm{Yb}^+$ $^2S_{1/2}-{}^2P_{1/2}$ resonance transition at $\lambda=369.5$ nm. The generated harmonic light has a maximum power of 10 $\mu$W and a bandwidth of less than 0.5 MHz [32]. During measurements, the optical power applied to the trap is reduced to approximately 2 $\mu$W, and the laser frequency is actively stabilized in order to maintain a constant detuning from the line center of the $F=1-F=0$ transition. A light field resonant with the $F=0-F=1$ hyperfine repumping transition is generated by modulating the injection current of the diode laser [33] at a frequency near $\Delta_S+\Delta_P \cong 14.7$ GHz. By a suitable choice of the free spectral ranges of the extended laser diode cavity and of the frequency-doubling cavity, the induced weak intensity modulation is resonantly enhanced and imparted on the second-harmonic output. A relative sideband power of a few percent is obtained at $\lambda=369.5$ nm, which is sufficient to reduce the average dwell time of ions in the $F=0$ ground state to less than $10^{-4}$ s.

Another extended-cavity diode laser excites the $^2D_{3/2}(F=1)-{}^3[3/2]_{1/2}(F=0)$ transition at $\lambda=935.2$ nm. The laser frequency is kept in resonance with the transition to within $\pm 20$ MHz by locking to a temperature-stabilized reference cavity. Spurious incoherent diode laser emission in the frequency range of the $F=2-F=1$ hyperfine component is blocked by transmission through a Fabry-Perot etalon. At an applied power in the range of 100 $\mu$W, the $\lambda=935.2$ nm excitation depletes the $^2D_{3/2}(F=1)$ level nearly completely without significantly reducing dwell times in the $^2D_{3/2}(F=2)$ state.

Probe radiation at $\lambda=435.5$ nm is produced by second-harmonic generation using the $\lambda=871$ nm emission of an extended-cavity diode laser. The emission linewidth of the free-running laser is in the range of 20 kHz; line center frequency fluctuations in a 1-s measurement interval have a typical magnitude of 0.3 MHz. The $\mathrm{TEM}_{00}$ transverse-mode resonance of a Fabry-Perot cavity made of low thermal expansion glass [34] serves as the frequency reference for active stabilization and controlled detuning of the laser frequency. The employed reference cavity has a free spectral range of 2 GHz, a $\mathrm{TEM}_{00}$ reflectivity contrast of 20%, and a finesse of approximately $2\times10^4$ at $\lambda=871$ nm. For thermal isolation, the cavity is placed in an aluminum enclosure kept at a constant temperature of approximately 25 °C. For mechanical isolation, the enclosure and an attached fiber coupling and mode matching optic are suspended by two springs of 1-m length in a vacuum of less than $10^{-7}$ mbar. The light field incident on the reference cavity is phase modulated at a frequency of 1.1 MHz by an injection current modulation of the diode laser. The correlated intensity modulation of the light returning from the cavity is detected as an optical frequency discriminator signal [35]. The amplified and time-integrated discriminator signal controls the frequency of the $\lambda=871$ nm diode laser. This frequency control circuit has a loop gain of more than $10^7$ in the frequency range below 1 kHz, and a unity-gain frequency of approximately 0.3 MHz.

As indicated in Fig. 2, a fraction of approximately 10 $\mu$W of the $\lambda=871$ nm laser output is passed through an acousto-optical modulator (AOM 2) which introduces a variable frequency offset for tuning. The frequency-shifted light is coupled into a polarization-preserving optical fiber. In order to reduce the effective reflectivity of the fiber endface, it is cut at an oblique angle with the fiber axis. The other endface of the fiber is glued to a lens which provides transverse mode matching to the reference cavity. A $\lambda/4$ plate is placed in front of the cavity, so that the light reflected by the cavity propagates through the fiber mainly in a polarization direction orthogonal to that of the forward-propagating light. The realized fiber coupling scheme offers the advantage that environmentally induced pendulum motion of the reference cavity suspension does not lead to significant variations in optical coupling efficiency or to Doppler-effect frequency shifts of the light incident on the cavity [12,36].

The long-term stability of the effective resonance frequency of the reference cavity was determined using the absorption spectrum of the $^2S_{1/2}(F=0)-{}^2D_{3/2}(F=2,m_F=0)$ transition of a trapped $^{171}$Yb ion as the frequency reference. Measurements conducted under unchanged experimental conditions during a 90 day period indicate an average linear drift of $+0.06$ Hz/s of the light field that is frequency locked to a reference cavity resonance. Additional frequency drifts which are correlated with ambient temperature changes have a maximum magnitude of 0.2 Hz/s and lead to maximum

frequency excursions of $\pm 25$ kHz relative to the average drift. The observed average frequency drift rate is in agreement with other observations on the dimensional aging of the reference cavity material [36,37]. In the present experiment, additional drifts seem to be caused mainly by a spurious reflection off the coupling fiber endface adjacent to the reference cavity. Independent measurements indicate an unexpected large power reflectivity of the endface of approximately 2% which is presumably due to degradation of the optical contact between fiber and attached lens. The effective reflection resonance frequency of the reference cavity is shifted by the interference of the light fields reflected by reference cavity and fiber endface. As a result of the low resonance reflection contrast of the reference cavity, the maximum shift is comparable to the cavity linewidth. The actual size of the shift is determined by the interference phase, which is susceptible to ambient temperature changes and minute mechanical vibrations. One thus expects that fluctuations of the spurious interference phase contribute strongly to both the observed temperature-dependent frequency drift, and to the short-time laser frequency instabilities which seem to determine the resolution limit in the spectroscopy of the $^2S_{1/2}(F=0)-{}^2D_{3/2}(F=2)$ transition (see Sec. IV B).

## IV. EXPERIMENTAL RESULTS

### A. Quantum-jump fluorescence signal

Figure 3 illustrates the temporal variation of the resonance flurescence emission of a single trapped $^{171}$Yb ion for the case of continuous laser cooling, and for the case of repeated state preparation and probe excitation as described in Sec. II. In the measurements shown in Fig. 3, the cooling laser frequency is chosen such that the fluorescence scattering rate is approximately one-half of the resonant scattering rate. The detected photon flux is approximately $5\times 10^3\ \mathrm{s}^{-1}$ when the resonance fluorescence level is high; during dark times, the signal level is determined by stray light and by the dark signal of the photodetection.

The measurement of Fig. 3(a) is typical of the quantum-jump fluorescence signal that is observed if the $F=1-F=0$ and $F=0-F=1$ components of the resonance transition and the $^2D_{3/2}(F=1)-{}^3[3/2]_{1/2}(F=0)$ transition at $\lambda=935.2$ nm are excited continuously. As discussed in Sec. II, periods without fluorescence scattering are induced by spontaneous transitions to the $^2D_{3/2}(F=2)$ level. The observed average length of bright and dark intervals is in good agreement with rate equation calculations, and confirms an earlier measurement of the natural lifetime of the $^2D_{3/2}$ state [18,21]. The signal level fluctuations within bright and dark intervals are predominantly due to photodetection shot noise.

Figures 3(b) and 3(c) show resonance fluorescence signals for the cases when phases of cooling, state preparation, and probe excitation are alternated. The same excitation sequence is used in the spectroscopic measurements discussed below. The cooling light fields are periodically blocked and released by a rotating-wheel chopper. The total cycle time is 65 ms; the cooling light fields are blocked during half the cycle time. In order to prepare the trapped ion in the $F=0$ ground state, the hyperfine repumping sideband is switched off 10 ms after the cooling light is unblocked. The resulting fluorescence signal is shown in Fig. 3(b). A closer inspection of Fig. 3(b) indicates that in most excitation cycles the fluorescence emission ceases by hyperfine pumping before the cooling light is shut off. The incidental dark interval of approximately two cycle lengths is likely caused by a spontaneous transition to the $^2D_{3/2}(F=2)$ level. Figure 3(c) shows the fluorescence signal for the case that $\lambda=435.5$ nm probe light is applied alternating with the cooling excitation. Probe pulses of approximately 100-nW power and 1-ms duration are produced by an acousto-optical modulator (AOM1 in Fig. 2). The pulses are resonant with the recoilless component of the $^2S_{1/2}(F=0)-{}^2D_{3/2}(F=2,\ m_F=0)$ transition, and are applied immediately before the start of each cooling phase. Figure 3(c) indicates a substantial transition probability to the $^2D_{3/2}(F=2)$ level because the fluorescence emission is delayed or entirely suppressed in a large fraction of the registered excitation cycles.

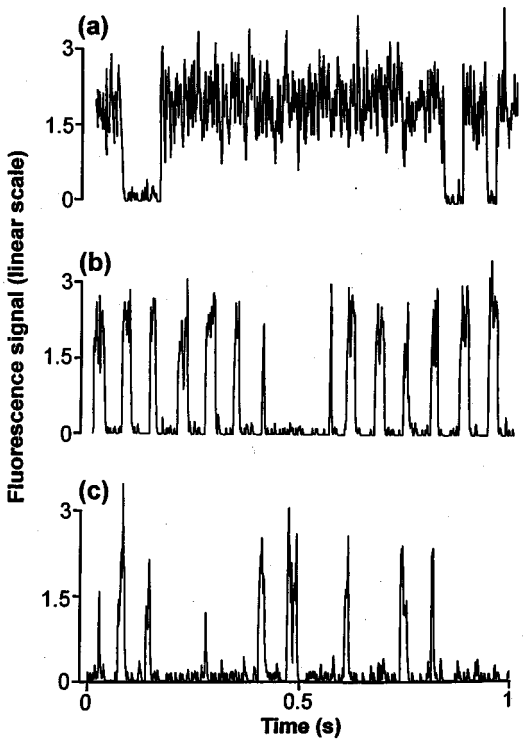


FIG. 3. Time-resolved resonance fluorescence emission of a trapped $^{171}$Yb ion. The displayed signal is the discriminated photomultiplier output pulse signal after passage through a low-pass filter with a 1-ms time constant. (a) Continuous cooling and hyperfine repumping excitation. (b) Cooling excitation periodically blocked; hyperfine repumping is applied only during the first part of each cooling phase. (c) $\lambda=435.5$ nm probe radiation is applied alternating with the cooling excitation; other conditions as in (b). The recording of signals (b) and (c) is synchronized with the unblocking of the cooling light. For further details, see the text.

### B. Spectroscopy of $^2S_{1/2}(F=0)-{}^2D_{3/2}(F=2)$ transition

Absorption spectra of the transition $^2S_{1/2}(F=0)-{}^2D_{3/2}(F=2)$ of a single trapped $^{17}$Yb ion were recorded

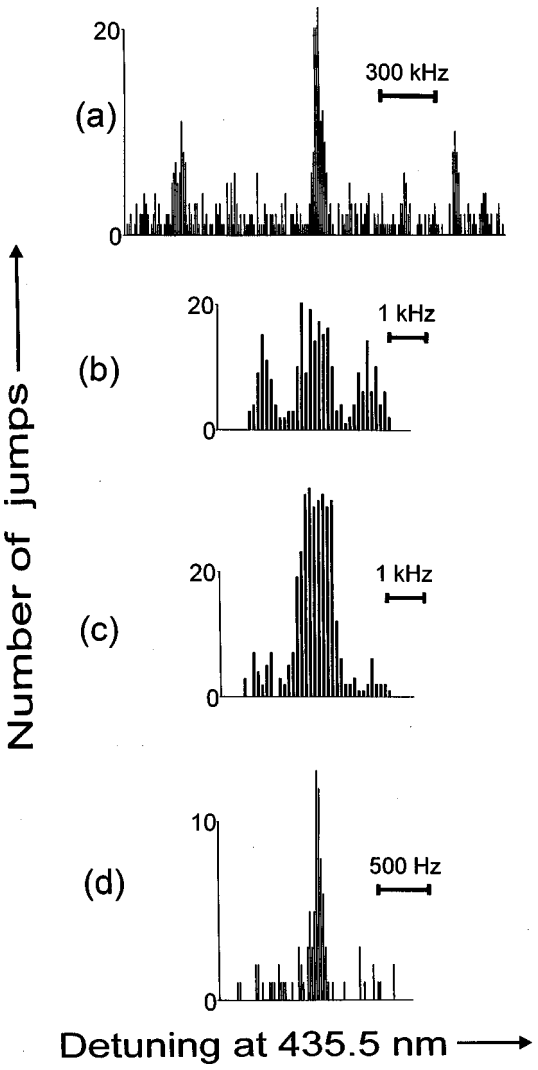


FIG. 4. Quantum-jump absorption spectra of the $^2S_{1/2}(F=0)-^2D_{3/2}(F=2,\ m_F=0)$ transition of a trapped $^{171}$Yb ion. The optical probe frequency at $\lambda=435.5$ nm increases from left to right according to the indicated scales. The vertical axes show the number of quantum jumps to the $^2D_{3/2}(F=2)$ level, which are counted for a given number $M$ of energy state measurements (see the text). (a) The probe frequency is incremented after $M=50$ measurements; the probe pulse length $\tau=1$ msec, the probe power is 1 $\mu$W. (b) $M=50$, $\tau=1$ ms, and the power is 50 nW. (c) $M=50$, $\tau=1$ ms, and the power is 25 nW. (d) $M=20$, $\tau=20$ ms, and the power is 0.5 nW.

using the excitation and detection scheme described in Sec. II. A fluorescence signal integration time of 3 ms is used to determine the atomic energy state after probe excitations. Unless noted otherwise, the time between the end of the probe pulse and the start of the cooling and detection phase is 1 ms.

The spectrum of Fig. 4(a) covers the frequency range of the recoilless carrier resonance and of the first-order secular-vibration sidebands of the transition to the $^2D_{3/2}(F=2,\ m_F=0)$ level. In order to reduce the number of data points required for the scan, the linewidth of the probe radiation was broadened to approximately 50 kHz by noise modulation of the probe laser frequency. The relative strength of the vibrational sideband structure was enhanced by a partial saturation of the carrier resonance. The radial vibration sidebands appear at a separation of approximately $\pm 730$ kHz from the carrier. The frequency difference between the two nearly degenerate radial sidebands is not resolved under the conditions of the measurement. The axial sidebands whose frequency separation from the carrier is approximately $\pm 870$ kHz are barely visible in Fig. 4(a), since their strength is comparable to the background noise level. The weak resonance signals which appear at approximately $\pm 500$ kHz from the carrier are artifacts produced by the active stabilization of the probe laser frequency. The observed frequency-independent background of quantum jumps is caused by spurious broadband emission of the probe laser and by spontaneous transitions to the $^2D_{3/2}(F=2)$ state, as discussed in Sec. II.

Figure 4(a) demonstrates confinement in the Lamb-Dicke regime since the vibrational sideband spectrum is dominated by the central carrier resonance. If the probe pulse power is reduced, the relative sideband strength decreases further and approaches the value expected at the Doppler cooling limit (see Table I). Measurements as shown in Fig. 4(a) were also performed for the case that the probe pulse was applied immediately after blocking of the cooling light, which reduces the average time between the stop of laser cooling and probe excitation by approximately 30 ms. Within the achieved signal-to-noise ratio, no significant change in relative vibrational sideband strength is observed. This allows to estimate an upper limit of the heating rate of the trapped ion in the absence of laser cooling. The inferred heating rate limit is $\partial\langle n^*\rangle/\partial t < 300\ \mathrm{s}^{-1}$, where $n^*$ denotes the effective quantum number of the observed projection of axial and radial vibration modes. Other experiments on single ions in rf traps have observed secular-vibration heating rates ranging from $\partial\langle n\rangle/\partial t \approx 1\ \mathrm{s}^{-1}$ to $\partial\langle n\rangle/\partial t \approx 10^3\ \mathrm{s}^{-1}$ [38,39].

High-resolution spectra of the carrier resonance of the vibrational spectrum are shown in Figs. 4(b)–4(d). The data collection time for each measurement was in the range of 90–150 s, which is sufficiently short to avoid significant line-shape distortions due to probe laser frequency drift. Figures 4(b) and 4(c) show the resonance signal under conditions where the Rabi sideband structure associated with saturated square-wave pulse excitation could be resolved [22]. The comparison with calculated transition probability line shapes indicates that the effective probe pulse area is approximately $3\pi/2$ in Fig. 4(b), and is close to $\pi$ in Fig. 4(c). The linewidth of the resonance peak of Fig. 4(c) is $\Delta\nu \cong 0.95$ kHz, in good agreement with the value $\Delta\nu \cong 0.8/\tau = 0.8$ kHz expected for excitation by a $\pi$ pulse of length $\tau = 1$ ms [22]. The observed maximum quantum jump probability, $P \cong 0.65$ in Fig. 4(c), appears to be limited mainly by fluctuations of the probe pulse area. Under the conditions of the experiment, substantial variations of the effective pulse area are introduced by probe laser frequency fluctuations and by the quantum-statistical fluctuation of the secular-vibration amplitude [12].

The Rabi sideband structure is not clearly resolved for probe pulse lengths of more than a few milliseconds. In the

limit of low power, linewidths of $\Delta\nu \cong 1/\tau$ are obtained for $1\,\text{ms} \leqslant \tau \leqslant 10\,\text{ms}$. For $\tau > 10\,\text{ms}$ the linewidth approaches a minimum value of typically $\Delta\nu \cong 80\,\text{Hz}$. A corresponding measurement is shown in Fig. 4(d); smaller linewidths in the range of $\Delta\nu \cong 50\,\text{Hz}$ were observed on a few occasions. It seems likely that the experimental linewidth minimum is determined mainly by probe laser frequency instabilities and not by fluctuations of the atomic resonance frequency. Under the conditions of the experiment, the estimated maximum short-time variation of confinement-related transition frequency shifts is negligible relative to the natural transition linewidth of 3.1 Hz [40,41]. The quadratic Zeeman frequency shift coefficient of the $^2S_{1/2}(F=0)-{}^2D_{3/2}(F=2, m_F=0)$ transition is calculated as $\delta\nu/B^2 \cong 52\,\text{kHz}/(\text{mT})^2$, where $B$ is the applied static magnetic field. In our case, $B \cong 0.25\,\text{mT}$, so that $\delta\nu \cong 3.2\,\text{kHz}$. The expected temporal variation of $\delta\nu$ due to the measured ambient alternating magnetic field is approximately $\pm 5$ Hz. The resulting frequency-modulation sideband structure is too weak to be resolved in the present experiment. The sensitivity of the $^{171}Yb^+$ transition frequency to magnetic-field variations could be further reduced by switching off the applied static magnetic field during probe intervals. Alternatively, optical pumping during laser cooling could be avoided by rapid polarization modulation of the laser-cooling light rather than by application of a static magnetic field [11,42].

### C. High-resolution vibration sideband spectrum

Imperfect temporal coherence of the ion vibration in the trap potential leads to a broadening of the secular-vibration sidebands relative to the carrier resonance. In the limit of low saturation, and for classical motion which satisfies the Lamb-Dicke condition, the broadening is proportional to $\Gamma_c = 1/\tau_c$, where $\tau_c$ is the effective first-order coherence time of the probed velocity oscillation [5]. The decoherence rate $\Gamma_c$ denotes the rate at which the coherence of the secular vibration decays due to fluctuations of the motional phase. For first-order vibration sidebands, the corresponding line broadening contribution is given by [5] $\Delta\nu = \Gamma_c/\pi$. Typically considered sources of motional decoherence include thermal heating by collisions or fluctuating electric fields, and fluctuations of the trap potential strength [24,25]. For decoherence caused by thermal heating, the order of magnitude of $\Gamma_c$ is given by the rate of the relative change in kinetic energy. Thus, if thermal heating were the dominant source of motional decoherence in the present experiment, the estimated heating rate limit (see Sec. IV B) would imply a decoherence rate limit of $\Gamma_c \approx \langle n^* \rangle^{-1} \partial\langle n^* \rangle/\partial t \leqslant 20\,\text{s}^{-1}$, corresponding to a broadening contribution of $\Delta\nu < 60\,\text{Hz}$ for the first-order vibrational sidebands.

A high-resolution secular-vibration spectrum obtained under experimental conditions similar to those of Figs. 4(b)–4(d) is shown in Fig. 5. The frequency differences between the three vibration modes are well resolved. The small frequency separation between the two radial modes indicates the degree to which the generated trap potential deviates from cylindrical symmetry as a result of incidental asymmetries of the trap electrode arrangement. The larger frequency

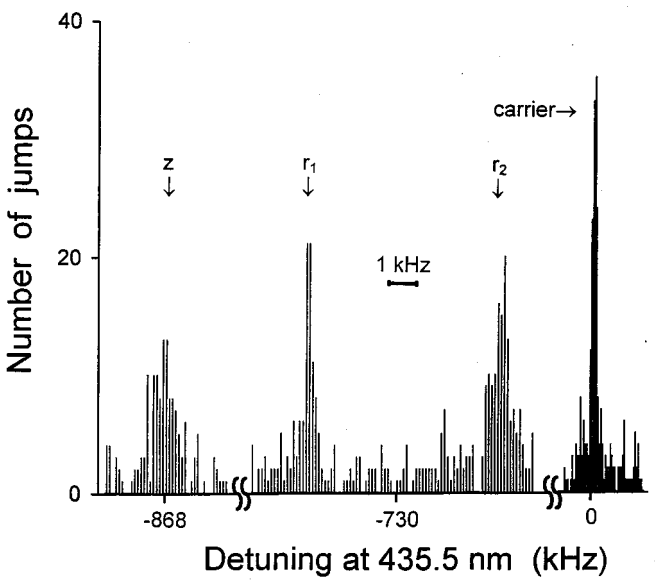


FIG. 5. High-resolution secular-vibration sideband spectrum of the $^2S_{1/2}(F=0)-{}^2D_{3/2}(F=2, m_F=0)$ transition of a trapped $^{171}Yb$ ion, showing first-order low-frequency sidebands associated with axial ($z$) and radial vibration modes ($r_1, r_2$). The origin of the detuning scale is at the carrier resonance which is also shown for comparison. Using a measurement scheme as in Figs. 4(a)–4(d) axial and radial sidebands and the carrier were recorded in separate frequency scans. The probe frequency is incremented after $M=50$ measurements, the probe pulse length is $\tau = 5\,\text{ms}$, and the probe pulse powers are 200 nW (sidebands) and 10 nW (carrier).

difference between axial and radial modes is determined by the choice of the trap operating parameters.

In the measurements shown in Fig. 5, saturation broadening was avoided by suitable choice of the employed probe pulse power. The linewidths of the sidebands did not change significantly when the probe pulse length was increased. The linewidths of $\Delta\nu \cong 0.2\,\text{kHz}$ obtained for the carrier resonance and for the sideband of the radial mode $r_1$ are not much larger than expected for $\pi$-pulse excitation with an employed pulse length $\tau = 5\,\text{ms}$. Linewidths of approximately $\Delta\nu \cong 1\,\text{kHz}$ are obtained for the sidebands of the axial mode and of the radial mode $r_2$. Assuming that the observed sideband linewidths are essentially determined by the decoherence of the secular vibration, the inferred effective motional decoherence rates are $\Gamma_c \approx 0.6 \times 10^3\,\text{s}^{-1}$ for the radial vibration mode $r_1$, and $\Gamma_c \approx 3 \times 10^3\,\text{s}^{-1}$ for the axial mode and the radial mode $r_2$.

The experimentally determined motional decoherence rates are considerably larger than the estimated maximum decoherence rate due to thermal heating. It thus appears that thermal heating is not a main source of motional decoherence in the present experiment. It is also unlikely that fluctuations of the trap potential depth are the only relevant decoherence source, since such fluctuations would give rise to essentially equal decoherence rates in the nearly degenerate radial modes. It appears difficult to gain a conclusive interpretation of the observed decoherence rate difference because the angular orientation of the radial vibration modes is

not known for the employed trap system. A vibration mode whose projection on the propagation direction of the cooling laser field nearly vanishes is not efficiently cooled so that the vibration amplitude can be significantly above the Doppler limit. Since in our case cooling and probe beams are collinear, the enhanced vibration amplitude would not be detected through a corresponding increase in the vibrational sideband strength. A significant vibration amplitude difference between the radial modes could, however, lead to different effective motional decoherence rates. The small frequency separation between the radial vibration modes can lead to additional experimental complications because nonlinear mode coupling by trap potential anharmonicities would receive a strong resonance enhancement.

## V. OUTLOOK

We have introduced and demonstrated an experimental scheme for high-resolution spectroscopy of the electric-quadrupole transition $^2S_{1/2}(F=0)-{}^2D_{3/2}(F=2)$ of trapped $^{171}Yb^+$. The recoilless resonance of the transition to the $m_F=0$ sublevel of the $^2D_{3/2}(F=2)$ state was resolved with a minimum linewidth of 80 Hz. The available frequency resolution was used to provide information on the motional decoherence characteristic of the employed trap system.

In order to utilize the $^2S_{1/2}(F=0)-{}^2D_{3/2}(F=2)$ transition of $^{171}Yb^+$ as an optical frequency standard, the transition frequency must be measured relative to an established frequency reference such as the cesium microwave frequency standard. Absolute transition frequency measurements on trapped ions based on phase-coherent optical frequency synthesis chains have so far been reported only for $Sr^+$ and $In^+$, with relative uncertainties of $5\times10^{-13}$ and $3\times10^{-11}$, respectively [41,16]. A measurement of the $^{171}Yb^+$ $^2S_{1/2}(F=0)-{}^2D_{3/2}(F=2)$ transition frequency could take advantage of the fact that the $Yb^+$ frequency can be linked relatively easily to the $^3P_1-{}^1S_0$ transition frequency of atomic calcium, which has been measured with a relative statistical uncertainty of less than $10^{-14}$ [43]. The measurement of the $Yb^+$ frequency is facilitated by the coincidence that the ratio of the $Yb^+$ and Ca transition frequencies deviates by only 0.6% from the simple integer ratio 3/2.

A prerequisite for the realization of a trapped-ion optical frequency standard is the evaluation of confinement-related shifts of the atomic transition frequency. In order to determine and minimize second-order Doppler and Stark-effect frequency shifts caused by trap field imperfections, it is usually necessary to measure the amplitude of the ion motion at the frequency of the trap field in three dimensions [31]. Due to the nonvanishing electric quadrupole moment of the $^2D_{3/2}(F=2)$ state of $^{171}Yb^+$, the magnetic sublevels of this state experience quadrupole shifts which are to first order proportional to the local electric field gradient. As discussed for $^{199}Hg^+$, the size of the linear quadrupole shift can be determined by variation of the orientation of the quantizing magnetic field [44]. One expects that the first-order quadrupole shift due to the trap field gradient vanishes if the trap field has no constant component. The second-order quadrupole shift by the trap field can be reduced to an estimated magnitude of less than 1 mHz by a suitable choice of the experimental geometry [13]. A quadrupole shift of order 0.1 Hz can result from uncompensated surface potential inhomogeneities of the trap electrodes [45].

Optical frequency standards based on electric-quadrupole transitions in single trapped alkalilike ions can ultimately reach a relative accuracy in the $10^{-18}$ range if transition frequency shifts due to ion motion are reduced to the minimum obtainable by laser cooling to the Doppler limit [1,3,43]. How well this condition is realized in a given experimental system is most clearly indicated by a systematic investigation of the dependence of the transition frequency on confinement conditions. The sensitivity of such measurements is generally determined mainly by the long-term stability of the employed frequency reference and by the achieved frequency resolution. An adequate reference for transition frequency shift investigations is obtained if two trap systems are operated simultaneously [46]. Due to recent progress in the development of tunable laser sources with extreme short-time frequency stability [47], it appears that optical spectroscopy on trapped ions with a relative frequency resolution in the $10^{-16}$ range will be feasible in the near future.

## ACKNOWLEDGMENTS

The authors are indebted to D. Griebsch for the construction of the trap system and of parts of the reference cavity system, and to F. Riehle for his critical reading of the manuscript. Part of this work was supported by Deutsche Forschungsgemeinschaft.

[1] See, e.g., D. J. Wineland, Science **237**, 612 (1987).
[2] R. H. Dicke, Phys. Rev. **89**, 472 (1953).
[3] H. G. Dehmelt, IEEE Trans. Instrum. Meas. **IM-31**, 83 (1982).
[4] F. G. Major and G. Werth, Phys. Rev. Lett. **30**, 1155 (1973).
[5] L. S. Cutler, R. P. Giffard, and M. G. McGuire, Appl. Phys. B: Photophys. Laser Chem. **36**, 137 (1985).
[6] J. D. Prestage, R. L. Tjoelker, G. J. Dick, and L. Maleki, J. Mod. Opt. **39**, 221 (1992).
[7] R. Blatt, H. Schnatz, and G. Werth, Phys. Rev. Lett. **48**, 1601 (1982).
[8] R. Casdorff, V. Enders, R. Blatt, W. Neuhauser, and P. E. Toschek, Ann. Phys. (N.Y.) **48**, 41 (1991).
[9] Chr. Tamm, D. Schnier, and A. Bauch, Appl. Phys. B: Photophys. Laser Chem. **60**, 19 (1995).
[10] P. T. H. Fisk, Rep. Prog. Phys. **60**, 761 (1997).
[11] D. J. Berkeland, J. D. Miller, J. C. Bergquist, W. M. Itano, and D. J. Wineland, Phys. Rev. Lett. **80**, 2089 (1998).
[12] J. C. Bergquist, W. M. Itano, and D. J. Wineland, in *Frontiers in Laser Spectroscopy*, Proceedings of the International School of Physics ''Enrico Fermi,'' edited by T. W. Hänsch and M. Inguscio (North-Holland, Amsterdam, 1994), Course CXX, p. 359.

[13] N. Yu, X. Zhao, H. Dehmelt, and W. Nagourney, Phys. Rev. A **50**, 2738 (1994).
[14] B. Appasamy, I. Siemers, Y. Stalgies, J. Eschner, R. Blatt, W. Neuhauser, and P. E. Toschek, Appl. Phys. B: Photophys. Laser Chem. **60**, 473 (1995); H. C. Nägerl, W. Bechter, J. Eschner, F. Schmidt-Kaler, and R. Blatt, *ibid.* **66**, 603 (1998).
[15] J. E. Bernard, L. Marmet, and A. A. Madej, Opt. Commun. **150**, 170 (1998); G. P. Barwood, P. Gill, G. Huang, H. A. Klein, and W. R. C. Rowley, Opt. Commun. **151**, 50 (1998).
[16] J. von Zanthier, J. Abel, Th. Becker, M. Fries, E. Peik, H. Walther, R. Holzwarth, J. Reichert, Th. Udem, T. W. Hänsch, A. Yu. Nevsky, M. N. Skvortsov, and S. N. Bagayev, Opt. Commun. **166**, 57 (1999).
[17] W. F. Meggers, J. Res. Natl. Bur. Stand., Sect. A **71**, 396 (1967); D. Engelke, Ph.D. thesis, University of Hannover, 1997, and PTB-Bericht OPT-57 (Wirtschaffsverlag NW, Bremerhaven, Germany, 1998).
[18] Ch. Gerz, J. Roths, F. Vedel, and G. Werth, Z. Phys. D: At., Mol. Clusters **8**, 235 (1988).
[19] A. S. Bell, P. Gill, H. A. Klein, A. P. Levick, Chr. Tamm, and D. Schnier, Phys. Rev. A **44**, R20 (1991).
[20] M. Roberts, P. Taylor, G. P. Barwood, P. Gill, H. A. Klein, and W. R. C. Rowley, Phys. Rev. Lett. **78**, 1876 (1997); P. Taylor, M. Roberts, S. V. Gateva-Kostova, R. B. M. Clarke, G. P. Barwood, W. R. C. Rowley, and P. Gill, Phys. Rev. A **56**, 2699 (1997).
[21] D. Engelke and Chr. Tamm, Europhys. Lett. **33**, 347 (1996).
[22] See, e.g., J. Vanier and C. Audoin, *The Quantum Physics of Atomic Frequency Standards* (Hilger, Bristol, 1989), p. 626.
[23] C. Monroe, D. M. Meekhof, B. E. King, and D. J. Wineland, Science **272**, 1131 (1996); D. M. Meekhof, C. Monroe, B. E. King, W. M. Itano, and D. J. Wineland, Phys. Rev. Lett. **76**, 1796 (1996).
[24] S. K. Lamoreaux, Phys. Rev. A **56**, 4970 (1997).
[25] M. Murao and P. L. Knight, Phys. Rev. A **58**, 663 (1998).
[26] B. C. Fawcett and M. Wilson, At. Data Nucl. Data Tables **47**, 241 (1991).
[27] W. M. Itano, J. C. Bergquist, J. J. Bollinger, J. M. Gilligan, D. J. Heinzen, F. L. Moore, M. G. Raizen, and D. J. Wineland, Phys. Rev. A **47**, 3554 (1993).
[28] R. Huesmann, Ch. Balzer, Ph. Courteille, W. Neuhauser, and P. E. Toschek, Phys. Rev. Lett. **82**, 1611 (1999).
[29] E. C. Beaty, J. Appl. Phys. **61**, 2118 (1987).
[30] K. Sugiyama and J. Yoda, Phys. Rev. A **55**, R10 (1997).
[31] D. J. Berkeland, J. D. Miller, J. C. Bergquist, W. M. Itano, and D. J. Wineland, J. Appl. Phys. **83**, 5025 (1998).
[32] Chr. Tamm, Appl. Phys. B: Photophys. Laser Chem. **56**, 295 (1993).
[33] C. J. Myatt, N. R. Newbury, and C. E. Wiemann, Opt. Lett. **18**, 649 (1993).
[34] Spacer and optically contacted mirror substrates are made of commercial-grade ultra-low expansion (ULE) glass material.
[35] R. W. P. Drever, J. L. Hall, F. V. Kowalski, J. Hough, G. M. Ford, A. J. Munley, and H. Ward, Appl. Phys. B: Photophys. Laser Chem. **31**, 97 (1983).
[36] L. Marmet, A. A. Madej, K. J. Siemsen, J. E. Bernard, and B. G. Whitford, IEEE Trans. Instrum. Meas. **46**, 169 (1997).
[37] G. P. Barwood, C. S. Edwards, P. Gill, G. Huang, H. A. Klein, and W. R. C. Rowley, IEEE Trans. Instrum. Meas. **44**, 117 (1995).
[38] F. Diedrich, J. C. Bergquist, W. M. Itano, and D. J. Wineland, Phys. Rev. Lett. **62**, 403 (1989).
[39] C. Monroe, D. M. Meekhof, B. E. King, S. R. Jefferts, W. M. Itano, D. J. Wineland, and P. Gould, Phys. Rev. Lett. **75**, 4011 (1995).
[40] D. J. Wineland, W. M. Itano, J. C. Bergquist, and R. G. Hulet, Phys. Rev. A **36**, 2220 (1987).
[41] J. E. Bernard, A. A. Madej, L. Marmet, B. G. Whitford, K. J. Siemsen, and S. Cundy, Phys. Rev. Lett. **82**, 3228 (1999).
[42] G. P. Barwood, P. Gill, H. A. Klein, and W. R. C. Rowley, in *Proceedings of the 5th Symposium on Frequency Standards and Metrology*, edited by J. C. Bergquist (World Scientific, Singapore, 1996), p. 503.
[43] H. Schnatz, B. Lipphardt, J. Helmcke, F. Riehle, and G. Zinner, Phys. Rev. Lett. **76**, 18 (1996); F. Riehle, H. Schnatz, B. Lipphardt, G. Zinner, T. Trebst, and J. Helmcke, in *Trapped Charged Particles and Fundamental Physics*, edited by D. H. E. Dubin and D. Schneider, AIP Conf. Proc. No. 457 (AIP, New York, 1999), p. 348.
[44] D. J. Wineland, J. C. Bergquist, W. M. Itano, F. Diedrich, and C. S. Weimer, in *The Hydrogen Atom*, edited by G. F. Bassani, M. Inguscio, and T. W. Hänsch (Springer-Verlag, Berlin, 1989), p. 123.
[45] M. Roberts, Ph.D. thesis, Imperial College and National Physical Laboratory, 1996.
[46] G. P. Barwood, G. Huang, H. A. Klein, P. Gill, and R. B. M. Clarke, Phys. Rev. A **59**, R3178 (1999).
[47] B. C. Young, F. C. Cruz, W. M. Itano, and J. C. Bergquist, Phys. Rev. Lett. **82**, 3799 (1999).